JOURNAL OF MATERIALS SCIENCE 31 (1996) 5529–5539

Observations on the formation of β-Al_5FeSi phase in 319 type Al–Si alloys

A. M. SAMUEL, F. H. SAMUEL,
Département des Sciences Appliquées, Université du Québec à Chicoutimi, 555, boulevard de l'Université, Chicoutimi (Québec), Canada G7H 2B1

H. W. DOTY
General Motors Corporation, NAO R and D Center, Metallurgy Department, 30500 Mound Road, Building 1-6, Warren, MI 48090, USA

In Al–Si alloys, the properties are influenced by the shape and distribution of the eutectic silicon particles in the matrix, as also by the iron intermetallics and copper phases that occur upon solidification. The β-Al_5FeSi iron intermetallic phase, in particular, is known for its detrimental effect on the properties, and is controlled variously by the iron content and the melt/solidification conditions of the alloy. The formation of the iron intermetallics has been observed in commercial 319 alloy end-chilled castings, obtained from non-treated and treated melts, where the effects of cooling rate, strontium modification and grain refinement have been studied. The volume fraction of β-phase formed was seen to increase with the decrease in cooling rate (i.e. with increasing distance from the chill) in the untreated alloy. Sympathetic (preferential) nucleation of the β-iron needles was also observed, in which the branching of β-needles from a parent needle resulted in the formation of large β-needle entities that can cover distances of ~1200 μm across the matrix surface. The beneficial effect of modification, i.e. strontium addition to the melt, was manifested through its influence on the fragmentation and dissolution of the β-needles. The strontium "poisons" the sites where sympathetic nucleation takes place. Dissolution was accelerated with increasing strontium content, the optimum level being ~300 p.p.m. Grain refining, on the other hand, negated the beneficial effect of modification, in that the β-needles underwent thickening and the sympathetic nucleation/branching also occurred. The modified alloy was found to possess the lowest volume fraction of β-Al_5FeSi phase among the unmodified, modified, grain-refined, and modified/grain-refined alloys.

1. Introduction

Premium quality Al–Si alloy castings of the type employed in automotive components require that effective control be exercised over both compositional and processing (i.e. melting, casting, heat treatment) parameters, in order to obtain optimum microstructural characteristics and, thereby, mechanical properties.

These microstructural characteristics, manifested variously in the grain size, dendrite arm spacing (DAS), type, shape and structure of the constituent phases, and the porosity distribution/profile, together influence the resulting properties, often in an interactive manner. The nature of the interaction can range from subtle to dominating, depending upon the elements or parameters in question.

In the particular case of 319 type Al–Si alloy, containing copper as the main alloying element and other elements as impurities, the mechanical properties are determined mainly by (a) the degree of supersaturation of copper and magnesium in the α-aluminium matrix, (b) the constituent phase particles, namely, the iron-intermetallics and copper phases that occur upon solidification, (c) the porosity size and distribution, as well as (d) the shape and distribution of the eutectic silicon particles in the matrix.

Depending upon the alloy composition, the iron intermetallics can occur in the α-$(Al_{15}(Fe,Mn)_3Si_2$ or Al_8Fe_2Si (in Al–Si–Mg alloy)), β-Al_5FeSi, or π-$Al_8FeMg_3Si_6$ forms, the β-phase being the one mainly responsible for the degradation in properties. According to Couture [1], although there is no unanimity amongst various sources in the literature as to the level of enhancement in mechanical properties obtained with the addition of iron, there is consensus, however, on its detrimental influence in the form of the β-phase. Existing as thin plates that appear as needles in the microstructure, the size of these β-needles is controlled by the composition and the solidification conditions of the alloy [2, 3].

The present article reports observations of the occurrence of β-Al_5FeSi needles in commercial 319.2

0022–2461

alloy, and forms part of an ongoing research programme covering detailed studies of the different aspects/parameters involved in the production and properties of 319 alloy castings. Eutectic silicon particle characteristics, porosity distribution, copper-phase dissolution and melting, and their effect on the tensile properties have been covered in earlier publications [4–6]. It was deemed pertinent to extend the investigation to include the effects of the melt-processing parameters, namely modification, grain refining and melt hydrogen level, and solidification conditions on the formation of iron intermetallics, in particular the β-phase, as a complement to these previous studies. The work reported here attempts to gain an understanding of the iron intermetallics observed in this important automotive alloy.

2. Experimental procedure

The chemical composition of the as-received 319.2 aluminium alloy is shown in Table I. The ingots were melted in a silicon carbide crucible of 7 kg capacity, using an electric resistance furnace. The melting temperature was held at 735 ± 5 °C. At this temperature, the molten metal was either degassed using high-purity argon (melt hydrogen content < 0.1 ml/100 g Al, designated H1) or gassed (hydrogen content ~0.37 ml/100 g Al, designated H3). The melt hydrogen level was monitored using an AlScan™ unit and was also determined from "Ransley" samples obtained from Ransley mould castings of each melt, using the Leco vacuum fusion technique.

Melts were also modified with strontium, added in levels of up to ~70–90, ~120–180, and ~250–310 p.p.m. (designated S1, S2, and S3, respectively) in the form of Al–10 wt % Sr master alloy, and grain refined by means of Al–Ti–B (Ti:B = 5:1) master alloy to obtain a 0.02 wt% titanium content (designated T).

Casting was done using a rectangular shaped end chill mould (with dimensions 64 mm × 127 mm × 254 mm), where the molten metal was poured through 8 pores cm^{-1} (i.e. 20 pores in^{-1}) ceramic foam filter discs fitted into the riser to avoid incident inclusions. Complete details of the mould and casting process are given elsewhere [5, 7]. Such an arrangement produced castings with solidification rates which decreased with increasing distance from the chill.

Samples were sectioned from the cast blocks in the horizontal orientation at varying heights above the water-chilled copper base, from which metallographic or tensile test sheet specimens were prepared. Table II indicates the average dendrite arm spacings (DASs) and local solidification times that were obtained corresponding to the different distances from the chill end in these castings.

TABLE I Chemical composition of the 319.2 and 319.1 alloys used in the present work

Alloy	Element (wt %)								
	Si	Cu	Fe	Mn	Mg	Ti	Zn	Ni	SF[b]
319.2[a]	6.23	3.77	0.46	0.14	0.06	0.073	0.08	0.008	0.74
319.1[a]	5.85	3.20	0.79	0.34	0.09	0.14	0.45	0.18	1.8

[a] Strontium content: ~0.0003 wt %.
[b] SF, Sludge factor.

TABLE II Variation in dendrite arm spacing and local solidification time as a function of distance from the chill end

Distance from the chill end (mm)	Local solidification time (s)	Average DAS (μm)
5	172	15
10	222	28
20	345	52
40	593	73
100	1222	95

Microstructural changes on polished surfaces of the metallographic samples (2 cm × 3 cm, cut from the central portion of the casting, at 5, 20, and 100 mm levels above the end chill bottom) were examined using optical microscopy. The α-aluminium dendrite arm spacings, eutectic silicon, and β-Al_5FeSi phase particle characteristics were analysed and quantified using a Leco 2001 image analyser in conjunction with the optical microscope (Olympus PMG3). Details of these measurements are given elsewhere [4].

In Section 3, it should be noted that reference is made in some cases to results obtained from 319.1 commercial alloy as well as experimental 319 alloys that were studied as part our research programme on 319 alloys. The chemical composition of 319.1 alloy is included in Table I, while specific elements for the experimental alloys are quoted in parentheses in each case throughout the text.

3. Results and discussion

In the context of the present work, prior to discussing the formation of the β-Al_5FeSi phase, it would be pertinent to recapitulate in brief the other aspects, namely porosity, eutectic silicon particle characteristics, DAS and tensile properties, of the 319.2 alloy castings (studied elsewhere), in order to present a comprehensive picture of the various factors involved in their production.

The interrelationships between DAS, porosity, and the tensile properties are summarized in Fig. 1. Fig. 1a, showing the variation in porosity volume percentage with DAS for degassed and filtered melt castings of the H1 alloys under the different melt treatment conditions, indicates the significant influence of DAS on porosity. The strength versus porosity and elongation versus porosity relations shown in Fig. 1b and c, respectively, reveal that while the ultimate tensile strength (UTS) and elongation (EL%) show a strong dependence on the porosity (their plots giving correlation coefficient (R^2) values of 0.78 and 0.80, respectively), the yield strength (YS) is apparently unaffected by the latter ($R^2 = 0.03$).

Fig. 2 shows the changes in the average silicon particle area (surface area as determined by the image analyser) and length in 319.2 alloy for different stron-

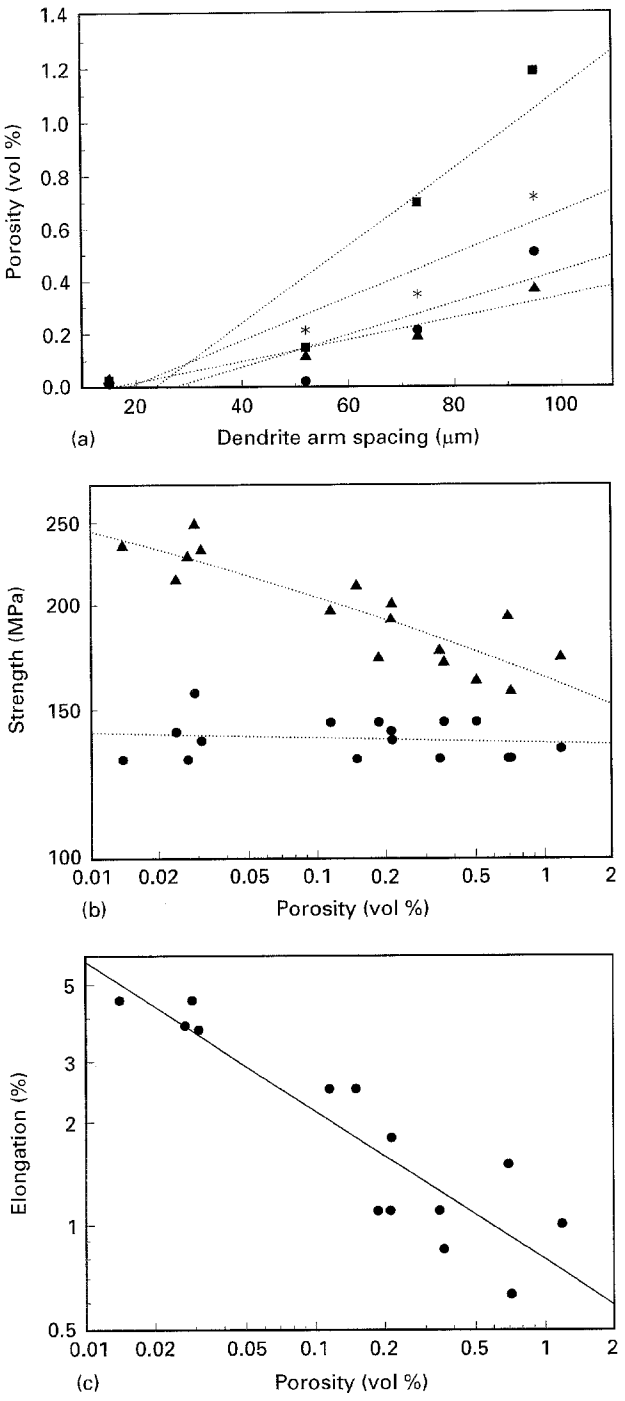

Figure 1 (a) Variation in porosity volume percentage with DAS for H1 alloys: (●) H1, (▲) H1T, (■) H1S3, (*) H1TS3. (b) Strength versus percentage porosity: (●) YS, (▲) UTS; and (c) (●) percentage elongation versus percentage porosity relations in 319.2 alloy.

tium additions. It can be seen that the silicon particle size is dependent on the α-aluminium DAS for the unmodified microstructure. Apparently, for such a low silicon (~6 wt%) and impurity content, an addition of ~90 p.p.m. strontium is sufficient to promote more or less complete modification of the silicon particles even at the lowest cooling rates (0.4 °C s^{-1}, DAS ~90 μm).

The plot of a DSC run carried out on a powdered sample of an experimental 319 alloy (containing 0.5 wt % Fe, 0.003 wt % Mg, DAS ~22 μm) is shown in Fig. 3, where the various points of interest (corresponding to the phases that will be discussed in the sections to follow) are delineated along the heating cycle part of the curve. The α/β phases occurring at

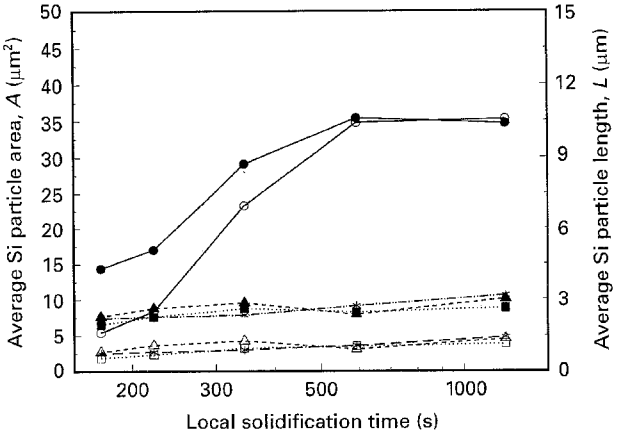

Figure 2 Variation in (—○—, --△--, --□--, --*--) average silicon particle area, *A* and (—●—, --▲--, --■--, --*--) average silicon particle length, L, as a function of local solidification time for various strontium concentrations: (○, ●) 10 p.p.m., (△, ▲) 90 p.p.m., (□, ■) 180 p.p.m. (*) 300 p.p.m.

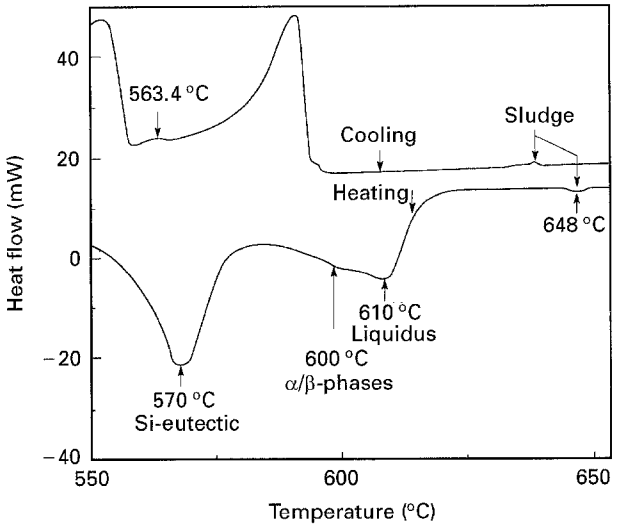

Figure 3 DSC plot of a powdered sample of an experimental 319 alloy (containing 0.5 wt % Fe, 0.003 wt % Mg, DAS ~22 μm), depicting the heating and cooling cycles in the temperature range 550–660 °C.

600 °C correspond to the α-iron and β-iron (Al_5FeSi) phases, respectively. Sludge formation is observed at a higher temperature, around 648 °C.

3.1. Formation and growth of β-Al_5FeSi phase needles

The use of very high cooling rates to produce finely distributed iron phases, or additions of trace elements to alter the morphology of the β-needles, are the means generally suggested to counteract the negative effect of iron [8]. Manganese and beryllium, as well as chromium and cobalt, are the "neutralizers" commonly employed. More recently, Awano and Shimizu [9] have proposed melt superheating as an alternative that dispenses with the use of neutralizing elements and results in the complete formation of the less harmful α-iron phase instead of the β-phase.

Narayanan *et al.* [10] have further investigated this phenomenon in 319 aluminium alloy and propose that the mechanism for the change in crystallization from

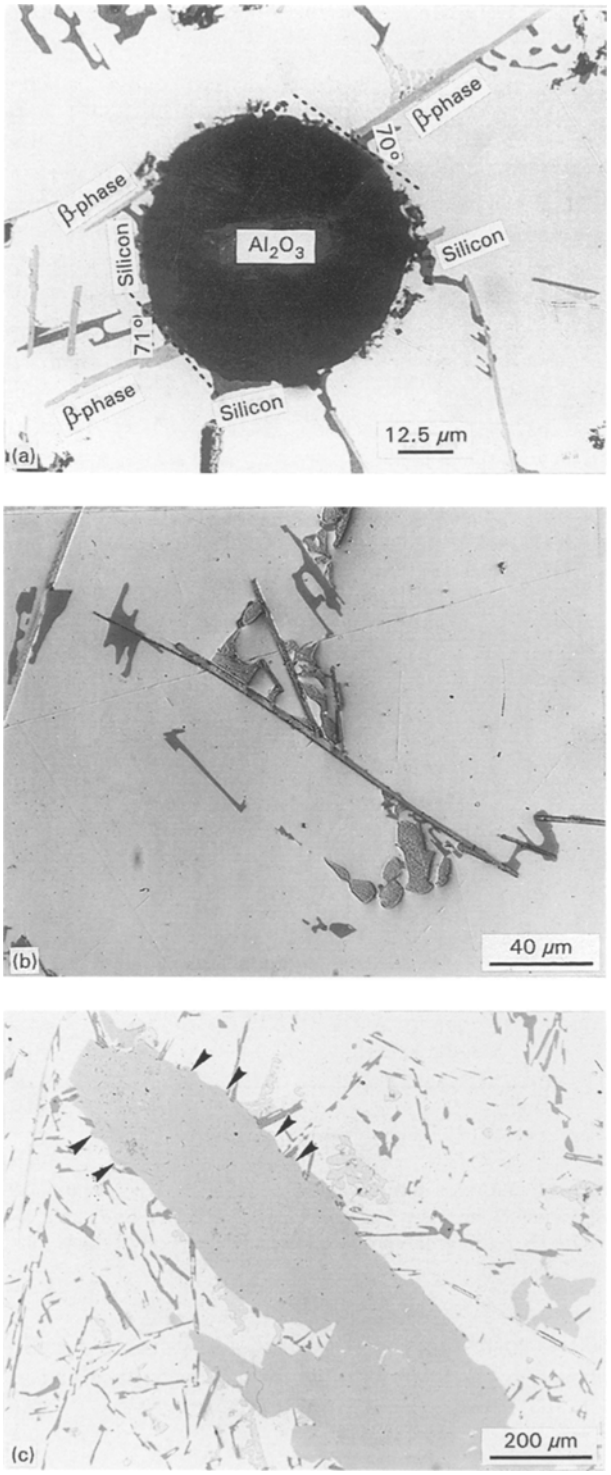

Figure 4 (a) Nucleation of β-Al_5FeSi needles on a γ-alumina particle in 319 alloy [10]. (b) Microstructure of H1 alloy showing the phenomenon of sympathetic nucleation of β-Al_5FeSi needles. (c) High-magnification micrograph of an experimental 319 alloy (containing 1% Fe and 0.14% Mn), showing growth of β-Al_5FeSi phase in the form of a large plate.

β- to α-AlFeSi upon melt superheating is related to the transformation of γ-aluminium oxide present in the melt to α-aluminium oxide at the high melt temperature, where the α-alumina, unlike the γ-variation, does not favour nucleation of the β-phase. The experimental results of alumina particle injection of 319 alloy carried out by these authors is depicted in Fig. 4a, where nucleation of β-Al_5FeSi needles on a γ-alumina particle can be observed, occurring approximately at an angle of 70° to the tangent of intersection with the alumina particle [10].

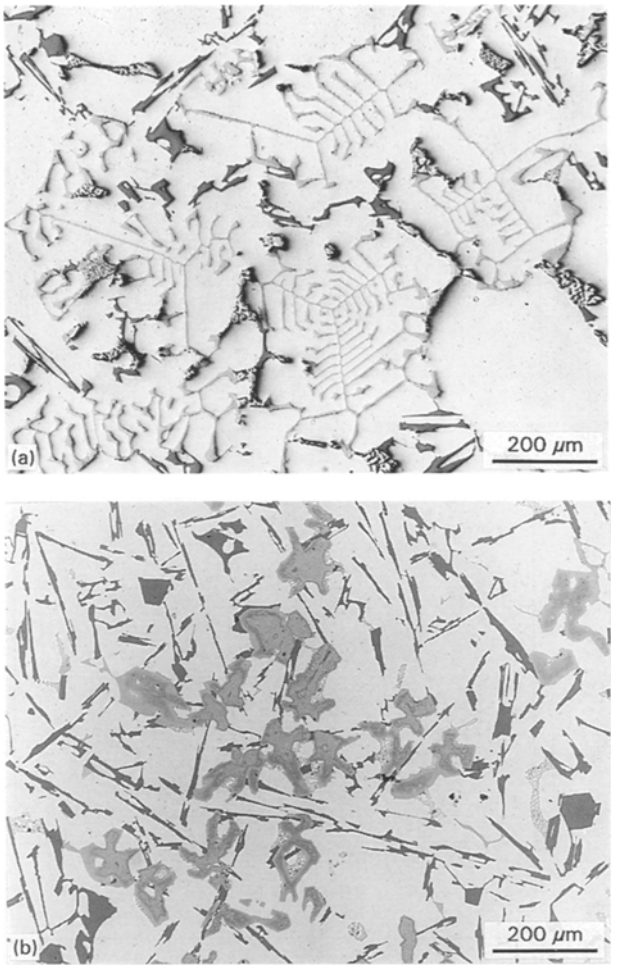

Figure 5 Microstructure of 319.1 alloy, showing (a) the presence of α-iron Chinese script phase, (b) evidence of sludge formation (light grey polyhedral shaped or star-shaped particles).

Fig. 4b is a microstructure obtained from the present alloy (an H1 alloy sample, corresponding to a DAS of ~70–90 μm), showing clearly the phenomenon of sympathetic nucleation commonly observed in the unmodified and grain-refined versions of the alloy. Smaller β-needles can be seen branching out from the parent needle spanning across the matrix surface. Close examination of the microstructure reveals that the smaller needles are indeed branches, and not two needles occurring one above the other and appearing to give the effect of branching when observed in a polished cross-section view of the alloy sample.

Fig. 4c is a high magnification micrograph of a 319 alloy sample (containing 1% Fe and 0.14% Mn), showing growth of the β-Al_5FeSi phase, where the normally needle-like structure has assumed large plate-like proportions. The growth appears to take place via a step-like motion of ledges, as highlighted by the arrows along the plate edge. Murali *et al.* [8] have also reported that in Al–7Si–0.3 Mg alloy with no trace additions, the β-phase is continuously present as plates at higher iron contents (> 0.6%).

The neutralizing influence of manganese addition can be observed in Fig. 5a which shows the microstructure of a 319.1 alloy sample. The microstructure is dominated by the presence of the Chinese script or

skeleton-like α-iron phase, and no β-needles are observed.

There are several mentions in the literature (see, for example, [1]) of the Fe–Mn effect in cast Al–Si and other aluminium alloys. In all cases, the "neutralization" consists of converting the iron-intermetallic from a brittle form (i.e. needles or platelets) to a less brittle or "relatively harmless" one (i.e. globular or Chinese script) that restores the tensile properties. The amount of manganese necessary to counteract a specified level of iron is quoted differently in different studies. Among some of the earlier investigations, Bonsack [11] has shown that the addition of 0.5% Mn to an Al–13%Si alloy containing 1.5% Fe transforms the β-needles into the Chinese script form.

Mascre [12] carried out metallographic studies on sand and permanent mould castings of the same alloy containing 0.55%–1.2% Fe and up to 1.3% Mn, and identified the existence of "m" or Al_5FeSi needles and a more compact "c" form of the iron compound whose presence was less detrimental to the properties. Based on contour plots obtained from the experimental data, he proposed a general formula of the type Mn% = 2(Fe% − 0.5) for the Fe–Mn neutralization effect. It is interesting to note that sodium modification was found to lower the iron level at which the "m" compound is primary and that the boundaries between the m and c phases depended on the cooling rate and the Fe/Mn ratio.

Colwell and Kissling [13] have also reported that addition of manganese in the ratio Mn:Fe = 1:2 breaks up the iron needles and ameliorates both the mechanical properties and castability of aluminium alloys. Following these and other studies, the general rule of thumb has been to keep the Fe:Mn ratio 2:1 in these alloys.

The addition of manganese can also result in the formation of a coarser variation of the α-phase, termed "sludge", that is usually observed in the bottom part of the melt, resulting from gravity segregation of this relatively dense constituent. Fig. 5b shows evidence of heavy sludge formation in the microstructure of a sample taken from the same 319.1 alloy, the sludge particles being the lighter grey polyhedrals or star-like shaped particles observed in the microstructure.

How much sludge may be formed is determined by how much iron, manganese and chromium exist in the alloy. Gobrecht [14] made an extensive study of sludge formation in several Al–Si casting alloys and used a segregation (or sludge) factor (SF) calculated as SF = 1(wt %Fe) + 2(wt %Mn) + 3(wt %Cr), to explore the relationship between temperature and composition in relation to sludge formation. Granger [15] has reported the star-like phase as having the formula $Al_{12}(Fe,Cr,Mn)_3Si_2$ in 339 alloy containing 0.06 wt % Cr, and assumed it to be derived from sludge ($Al_{15}(Fe,Mn)_3Si_2$).

3.2. Size and distribution of β-Al_5FeSi phase needles (image analysis)

3.2.1. Effect of cooling rate

Microstructures of H1 alloy taken from samples obtained at 5 and 100 mm above the chill end are shown in Fig. 6a and b, respectively. With the high cooling

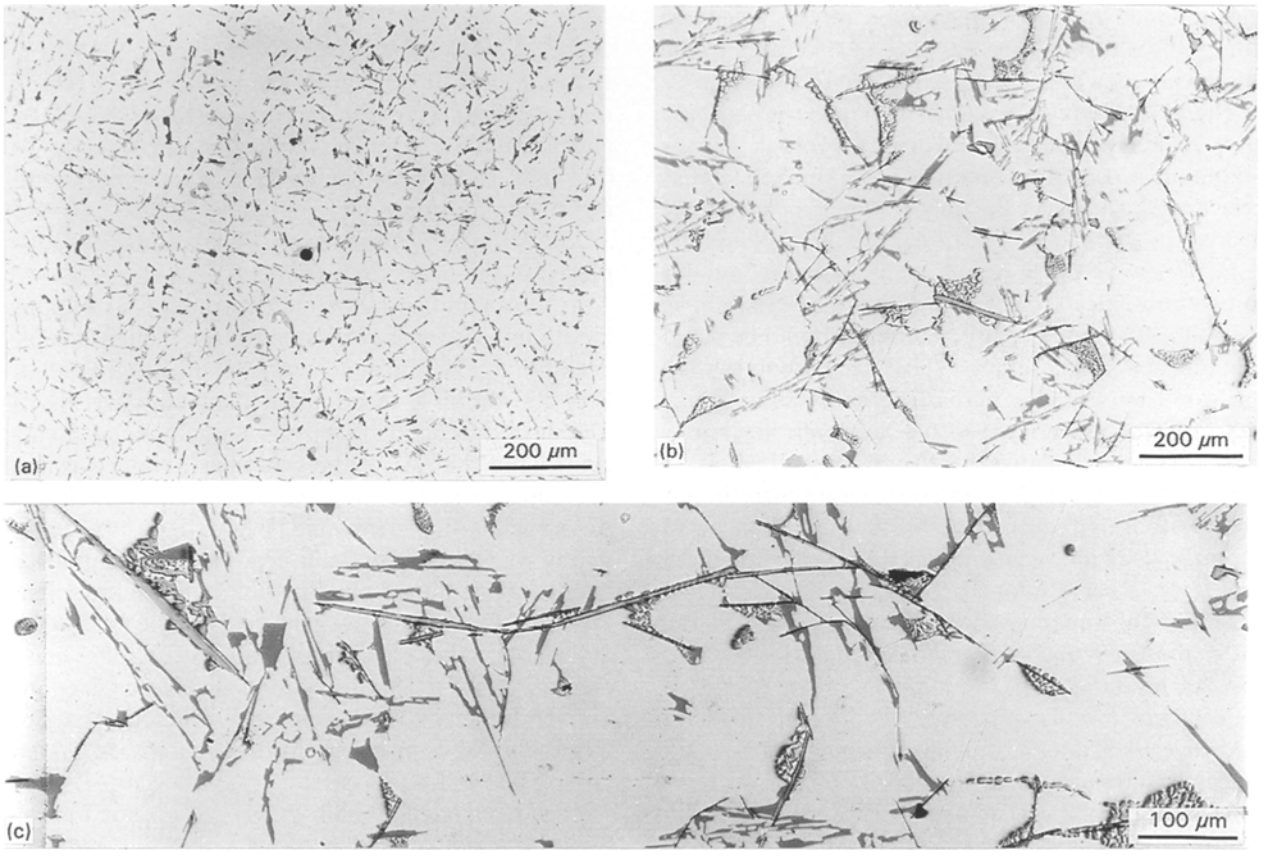

Figure 6 Microstructures of H1 alloy obtained at (a) 5 mm, and (b) 100 mm distance from the chill end; (c) high-magnification micrograph of (b) showing occurrence of sympathetic nucleation of β-Al_5FeSi needles extending across the matrix surface.

rate obtained at the 5 mm level, the microstructural constituents are very fine in size, and eutectic silicon particles, Al_2Cu eutectic phase and α-iron phase particles are easily detected. However, it was extremely difficult to discern the presence of β-needles at the ×100 magnification at which the observations were made, Fig. 6a. At the 100 mm level and at the same magnification, β-needles are observed in relative abundance, Fig. 6b. The eutectic copper phase is seen nucleating along the sides of the needles. Also, the effect of the difference in cooling rates on the size of the microconstituents is clearly visible.

Fig. 6c is a high magnification micrograph of the same alloy sample (at 100 mm), showing the occurrence of sympathetic (i.e. secondary) nucleation of β-needles which can extend by as much as 1200 μm across the matrix surface. Individual branches of β-needles range in size from 100–125 μm. It is important to note in this connection that the β-needle length measurements reported in the literature are usually the lengths of straight segments of these needles, preferably individual needles. Thus, a reported average maximum β-length could very well represent the average of such straight segments of β-needles. Given the fact that it is the lengths (and thickness) of these needles that are related to and determine the extent of degradation in properties, the possibility of the greater harmful effect of a network of sympathetically nucleated β-needles extending over large distances in the matrix should not be overlooked. One of the direct consequences that spring to mind is the effect on feedability of the alloy during casting.

It is important, therefore, to ensure that such sympathetically nucleated β-needle entities do not exist in the obtained microstructure. One of the means of doing this is through the addition of strontium to the alloy melt, as will be discussed in the next section.

The H1 alloy can be taken to represent the base alloy reference, where the hydrogen content is at its minimum possible, no modifier or grain refiner has been added, and hence the only parameter affecting the microstructure and its constituents is the cooling rate.

Fig. 7 shows the β-needle length range count for samples obtained at the 5, 20 and 100 mm levels above the chill end of an H1 alloy casting. It should be noted that for each sample, at least 100 β-needle lengths were measured by scanning across the entire sample surface, and the percentage of needles lying in various length ranges calculated therefrom. In contrast to the 5 mm level sample (whose microstructure corresponds to a DAS of ~15 μm) where all the β-needle lengths lie in the 0–25 μm length range, a variety of β-length ranges is observed for the 100 mm sample (DAS ~95 μm), the maximum centred around 100–150 μm, with almost equal amounts in the 50–100 and 150–200 μm ranges on either side. β-lengths as high as 450–500 μm are also observed. At the intermediary DAS level (~52 μm, 20 mm level sample), the β-length ranges are found centred around 20–50 μm, with almost equal numbers in the 0–25 and 50–100 μm ranges. No β-needles larger than 150 μm are observed.

Thus, the coarser the microstructure, the longer the lengths of the β-needles observed in the base H1 alloy.

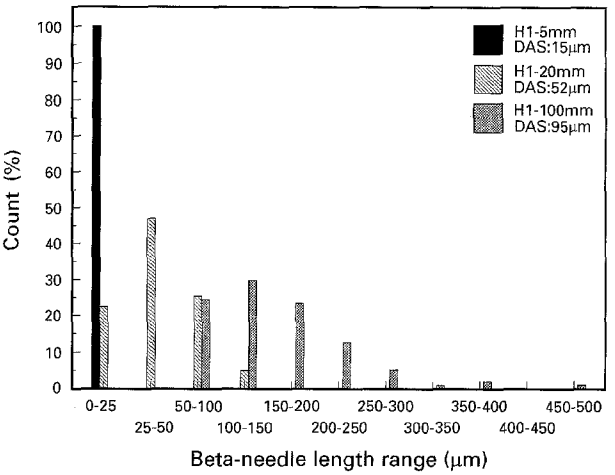

Figure 7 Histogram depicting the β-needle length range count for H1 alloy samples obtained at 5, 20, and 100 mm distance from the chill end.

Taking the length range giving a maximum count of β-needles in each case as representative of the average β-needle length observed at that particular DAS, the β-needle length approximately increases with the increase in DAS as 1:1:1.7.

In the following sections, the size and distribution of the β-needles formed under the different alloy conditions studied will be presented as histograms which will be compared with the H1 alloy reference to elucidate the effects of modifier, grain refiner or a combination of the two on the formation of the β-needles. As before, in each case at least 100 β-needle lengths were measured, covering the entire surface of the sample.

3.2.2. Effect of modification

In addition to the H1 alloy samples, β-needle length measurements were also carried out for H1S1, H1S2 and H1S3 alloy samples obtained at the three levels (5, 20 and 100 mm) as before, S1, S2 and S3 representing strontium additions of ~70–90, ~120–180 and ~250–310 p.p.m., respectively. The results are displayed in the histograms of Fig. 8.

At the 5 mm level, the β-needle length distributions in all samples are skewed toward the smaller lengths, peaking typically around the 5–10 μm length range. Broadly speaking, therefore, at the 5 mm level (DAS ~15 μm), the cooling rate is the main dominant factor controlling the size of the β-needles obtained in the microstructure, and not the amount of strontium. Nevertheless, it is interesting to note that the effect of strontium addition is manifested through its influence on the fragmentation and dissolution of the β-needles. Particularly at the sites where sympathetic nucleation of the latter takes place, the strontium "poisons" these nucleation sites. The dissolution of the needles into smaller fragments results in the higher counts observed for the lowest length range compared to the unmodified (H1 alloy) case.

At a distance of 20 mm (DAS ~52 μm) or further from the chill, the influence of strontium addition takes precedence over that of cooling rate. From the skewed profile observed for the H1 alloy sample, the

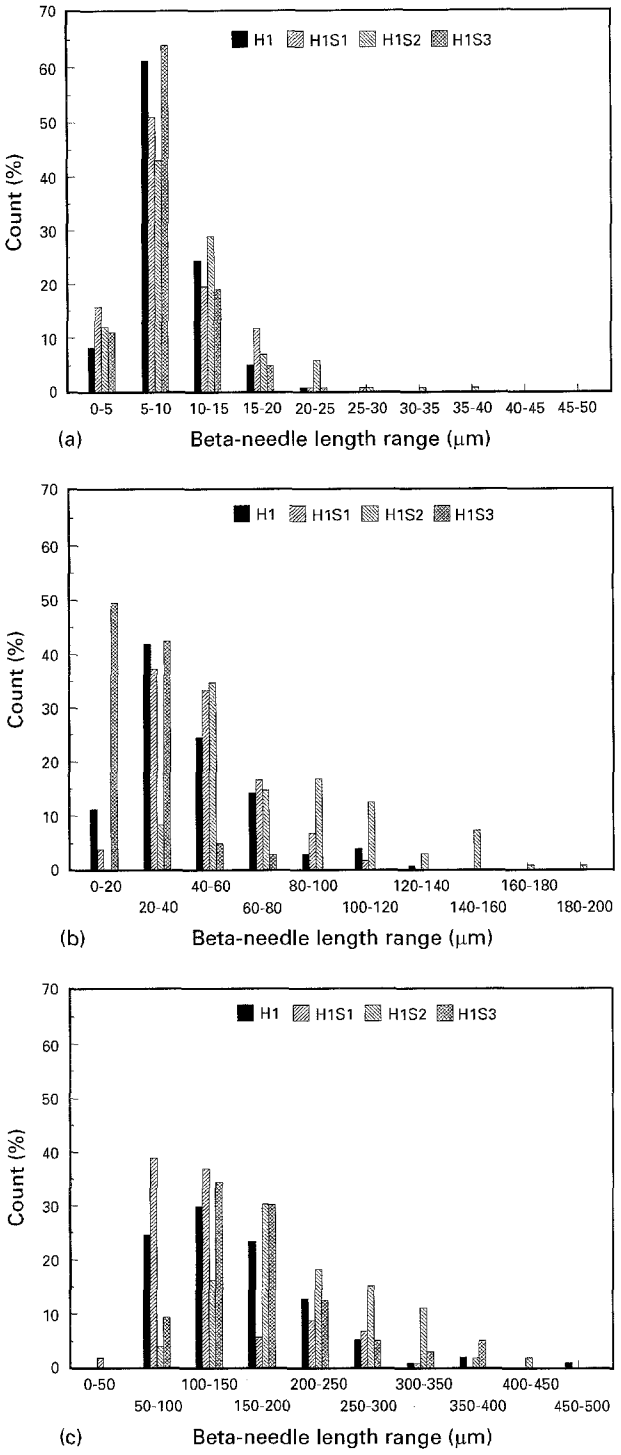

Figure 8 Histograms depicting β-needle length range counts for H1S1, H1S2 and H1S3 alloy samples obtained at (a) 5 mm (DAS 15 μm), (b) 20 mm (DAS 52 μm), and (c) 100 mm (DAS 95 μm) distance from the chill end.

addition of strontium gradually shifts the needle-length sizes to the right, towards larger lengths for H1S1 alloy. Increasing the strontium level to S2 further shifts the profile to the right towards still larger needle lengths. Compared to the maximum 120–140 μm range observed in H1 alloy, the β-needle lengths can go up to 180–200 μm in H1S2 alloy, whereas the S1 level of strontium addition produces no significant changes in length. On the contrary, at ~300 p.p.m. strontium level, almost 90% of the needles lie between 0 and 40 μm, compared to about 55% for H1 alloy, and the needle lengths do not exceed the 60–80 μm range.

Two points must be taken into consideration to explain this seeming discrepancy.

(i) Microstructural observations of these samples show that while sympathetic nucleation appears abundantly in the H1 alloy samples at the higher dendrite arm spacings, with the addition of strontium, the phenomenon is vastly reduced. The strontium poisons the nucleation sites of the β-needles. Consequently, the β-iron phase must precipitate at a smaller number of sites, resulting in the precipitation of needles that are larger compared to the branched segments of the sympathetically nucleated β-needle entities observed in the H1 alloy microstructure. The overall result, however, is that this reduces the total number of β-needles in a specified area and hence a smaller volume fraction of β-needles is obtained than in the case of the unmodified alloy.

If one were to take into consideration the total lengths of the sympathetically nucleated β-needles in the H1 alloy samples (as shown in Fig. 6c), however, its histogram would have a profile opposite to that shown in Fig. 8, with the maximum skewed to the right, towards the largest lengths. This procedure is probably not followed in most cases due to the cumbersome nature of such measurements, and to simplify matters, the measurements are restricted to straight β-needles, i.e. individual needles only, and not branched or curved β-needles that may be observed in the microstructure.

(ii) The addition of 300 p.p.m. strontium is seen to accelerate the dissolution process, with individual β-needle segments breaking up into two or more fragments that results in much higher counts observed in the lower β-length ranges for the H1S3 sample, and a reduction in maximum length to 60–80 μm (cf. 120–140 μm in the case of H1 alloy). This action of strontium is brought out even more forcefully if one compares the entire lengths (~1200 μm) of the β-needle entities observed in the H1 alloy samples with the latter.

Fig. 9 shows typical examples of the microstructures observed in H1S3 alloy samples obtained at 5 and 100 mm distance from the chill end. The very fine modified eutectic silicon structure produced by the 300 p.p.m. level of strontium is evident even at 100 mm distance from the chill, Fig. 9b. Also apparent in Fig. 9b are the β-needles, found existing mostly as individual needles (cf. the sympathetically nucleated entities observed in the corresponding H1 alloy sample, Fig. 6b). The presence of α-iron Chinese script phase is also noticed. It should be noted that with respect to these two forms of the iron phase, no major $\beta \rightarrow \alpha$ transformation was observed in the H1S3 alloy samples. In other words, the presence of strontium does not promote significant conversion of the β-iron to the α-iron phase as has been reported in the case of wrought aluminium alloys (1XXX series and 6061) by Mulazimoglu *et al.* [16].

Some of the interesting features observed in the H1S3-100 mm alloy sample are shown in Fig. 10. In Fig. 10a, sludge particles can be observed (open

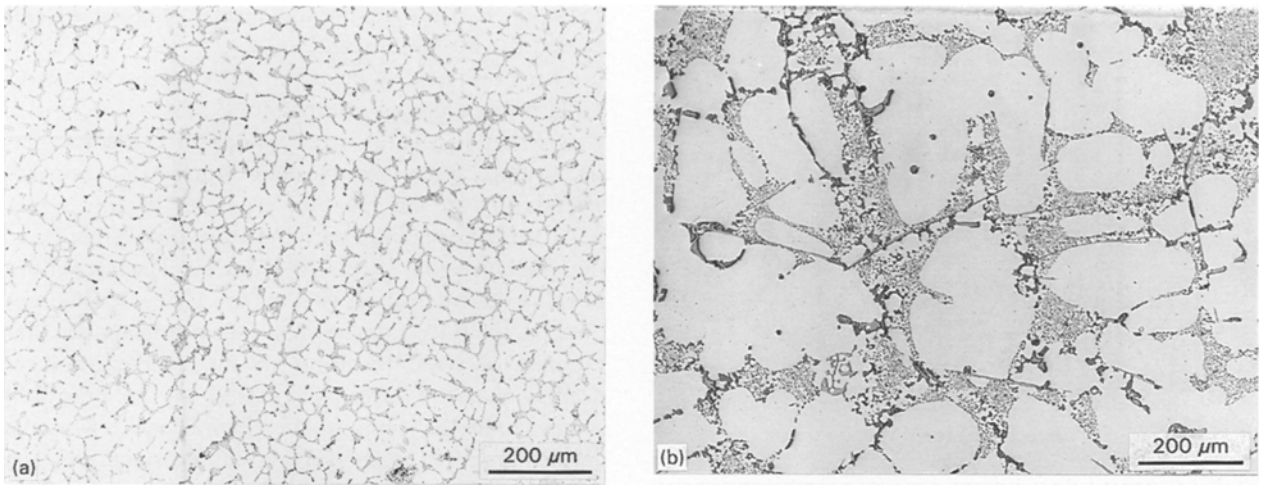

Figure 9 Microstructures of H1S3 alloy samples obtained at (a) 5 mm, (b) 100 mm distance from the chill end.

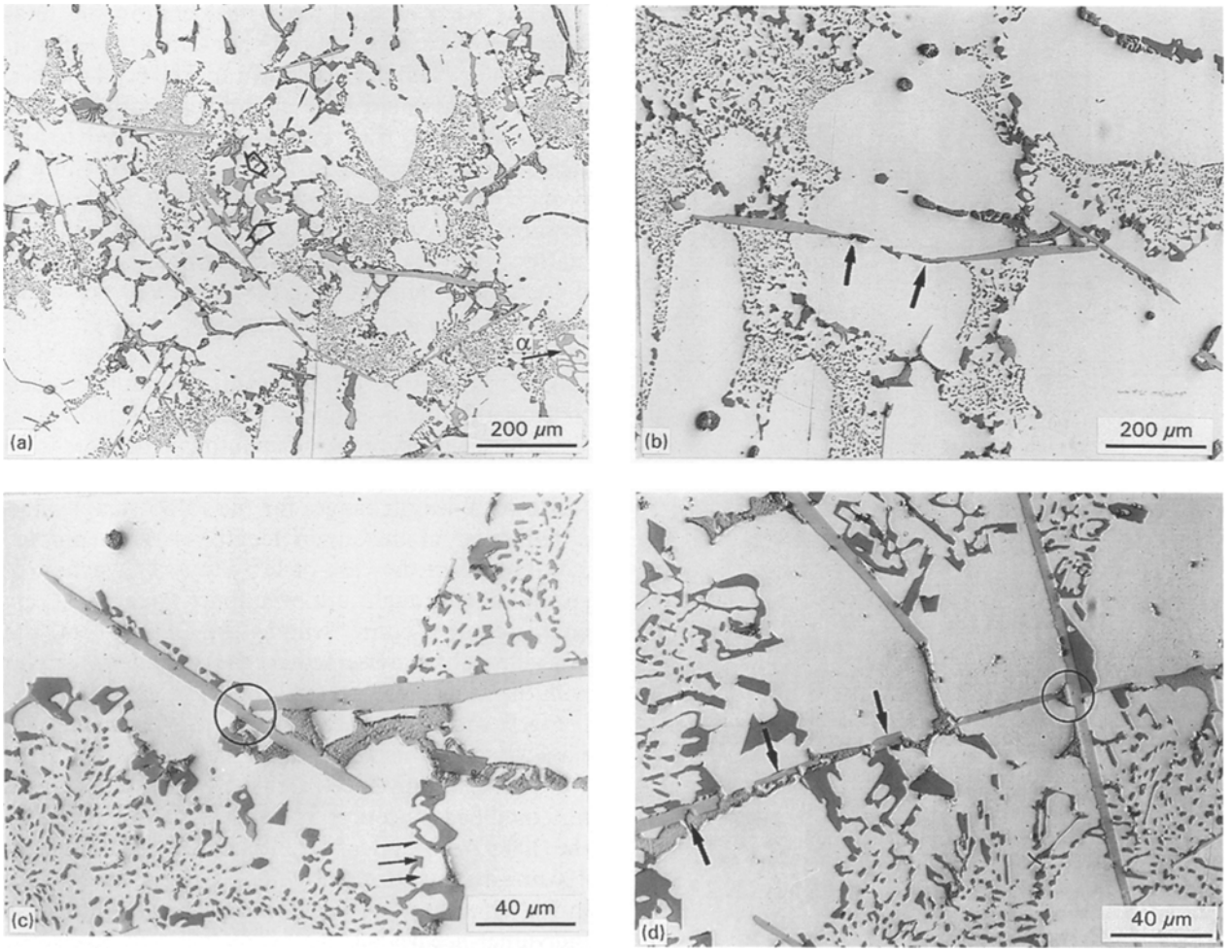

Figure 10 Microstructures of H1S3 alloy obtained at 100 mm distance from the chill end, showing (a) sludge particles (open arrows), β-Al_5FeSi needles and an α-iron Chinese script phase particle; (b) effect of strontium on the dissolution/fragmentation of β-needles (arrows show segments of a broken β-Al_5FeSi needle); (c) how strontium poisons the link between a parent and branching Al_5FeSi needle; (d) poisoning and dissolution/fragmentation effect of strontium on the β-needles.

arrows) in addition to the β-Al_5FeSi needles and the α-iron phase particle seen in the right-hand bottom corner. Such sludge particles were, generally, rarely observed in the microstructures. Fig. 10b shows the effect of strontium on the dissolution of the β-needles as marked by the arrows delineating the broken segments of a β-Al_5FeSi needle in the microstructure. In Fig. 10c, the "poisoning" effect of strontium on a nucleation site of the β-needle (see circled area showing the breaking of the link between parent and branching β-needles) can be clearly seen. Some overmodification of the silicon particles is also observed (arrowed). Fig. 10d shows a clear example of both the poisoning and dissolution effect of strontium on the β-needles.

The script-like particles observed in the microstructure are probably overmodified silicon particles, judging by their colour.

3.2.3. Effect of grain refining

Fig. 11a and b demonstrate the effect of grain refining on the β-needles. Microstructures obtained from H1T alloy at 100 mm distance above the chill end indicate a tendency for thickening of the β-needles. Fig. 11a shows the thickening takes place via the step-like motion of ledges mentioned earlier (Section 3.3.1), delineated by the small arrows. In Fig. 11b, fracture of the thicker branch is observed to occur, which is different from the fragmentation of the β-needles that results from strontium modification. The fractured parts indicate the brittle nature of the fracture.

Microstructures obtained from grain-refined H1S3 alloy (i.e. H1TS3 alloy) obtained at 100 mm distance from the chill are shown in Fig. 12. In Fig. 12a, one can observe branching and thickening of the β-needles. Sympathetic nucleation was observed more frequently in these samples (see the circled areas in Fig. 12b), compared to H1S3 alloy. The open arrow in Fig. 12b indicates the α-iron script form, one of the few instances when the phase was found to occur. Also observed is the Al_2Cu phase in the vicinity of the β-needles.

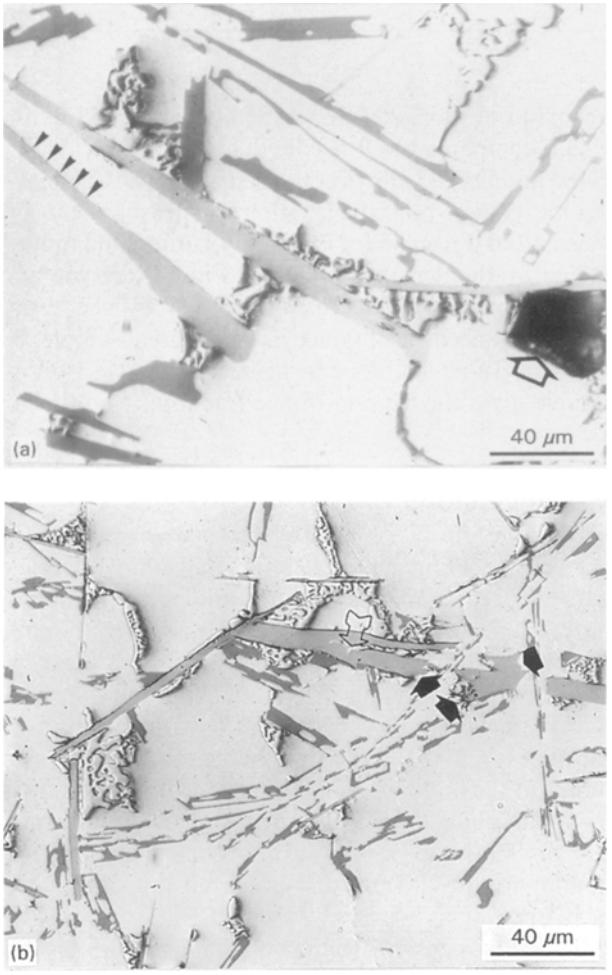

Figure 11 Microstructures of H1T alloy obtained at 100 mm distance from the chill end, showing (a) thickening of the β-Al_5FeSi needles that takes place via a step-like motion of ledges (arrowed), (b) fracture of a thick β-Al_5FeSi needle. Note the pore along the long side of the β-needle (open arrow) in (a).

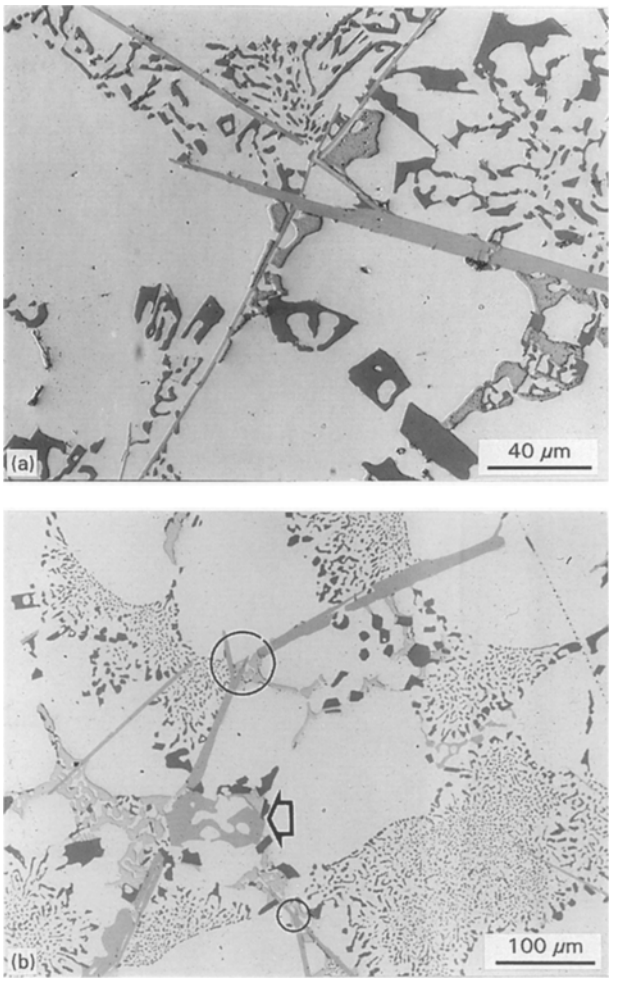

Figure 12 Microstructures obtained from H1TS3 alloy at 100 mm distance from the chill end, showing (a) branching and thickening of the β-needles, (b) sympathetic nucleation (circled areas) of β-needles and α-iron script phase (open arrow) and Al_2Cu phase in the vicinity of the β-needles.

The histograms of Fig. 13 compare the effects of grain refining, modification, and their combined effect on the number of β-needles observed in the respectively treated H1 alloy samples (namely, H1T, H1S3 and H1TS3) obtained at different levels above the chill end. At the smallest DAS (*i.e.* at 5 mm distance above the chill), grain refinement is seen to increase the lengths of the β-needles to larger sizes, whereas modification reduces their size compared to the base H1 alloy case. The latter observation is partly accounted for by the dissolution effect of the strontium on the β-needles. The combined effect of modification and grain refinement tends to produce a more rounded rather than skewed type of profile, mainly distributed across 10–25 μm, and tapering off on either end of this range.

As the dendrite arm spacing increases (i.e. at the 20 mm level), the dissolution effect of strontium again ameliorates the situation in the H1S3 sample compared to H1, with most β-needles being observed in the 0–40 μm range. H1T and H1TS3 alloys, however,

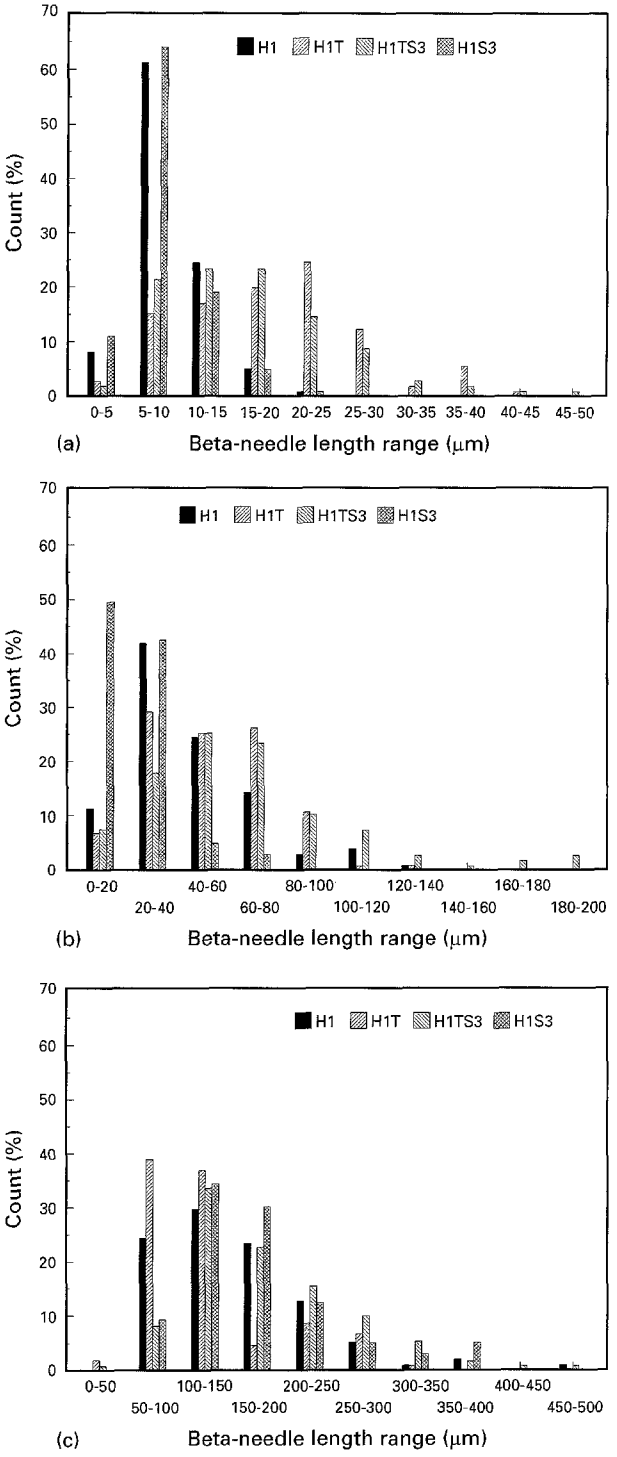

Figure 13 Histograms depicting the β-needle count in H1, H1T, H1S3 and H1TS3 alloys obtained at (a) 5 mm (DAS 15 μm), (b) 20 mm (DAS 52 μm), and (c) 100 mm (DAS 95 μm) distance from the chill end.

give almost the same results as before. In other words, the addition of grain refiner nullifies the beneficial effect obtained with strontium addition in H1S3 alloy. The microstructure of Fig. 10c gives evidence of this. At the largest DAS (i.e. at 100 mm distance from the chill), the H1T alloy sample apparently shows the maximum count of β-needles in the lowest ranges (50–150 μm). Calculating the density of β-needles in each of these samples over a constant sample surface area, it is found, however, that the H1T alloy has a much larger count of needles than H1S3 alloy (100 mm distance from the chill samples). This is

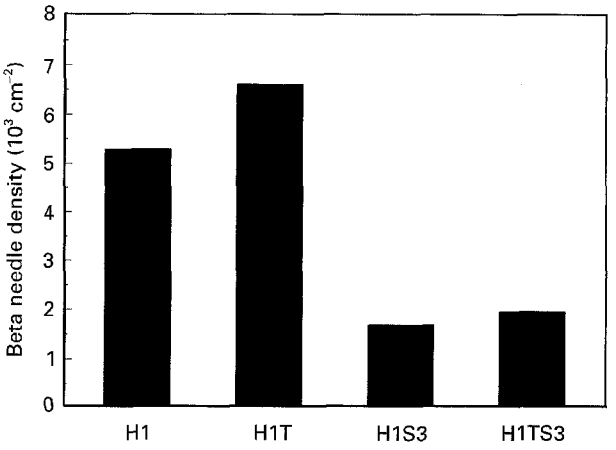

Figure 14 Histogram comparing β-needle densities of H1, H1T, H1S3 and H1TS3 alloy samples obtained at 100 mm (DAS 95 μm) distance from the chill end.

TABLE III β-Al_5FeSi statistics for H1 alloys (sample DAS ~ 95 μm)

Alloy	Average β-length (μm)	β-needle density (cm^{-2})	Total β-length (volume fraction) (10^5 μm cm^{-2})
H1	145	5310	7.70
H1T	118	6542	7.72
H1S3	175	1714	3.00
H1TS3	167	1958	3.27

brought out more clearly by the histogram of Fig. 14 which compares the β-needle densities for H1, H1T, H1S3 and H1TS3 alloys at the 100 mm level. Calculating the average β-needle length from measurements of at least 100 β-needles for each alloy sample, and multiplying by the densities shown in Fig. 14, the volume fraction of the β-phase (as measured by the total length of β-needles) obtained in the different samples is given in Table III. As can be seen, the H1S3 alloy sample gives the lowest volume fraction.

4. Conclusions

From our study of the occurrence of β-Al_5FeSi needles in commercial 319 end chill alloy castings with respect to microstructural and melt treatment parameters, the following conclusions may be summarized.

1. Cooling rate influences both the formation and size of the β-needles in the alloy, with hardly any β-needles being observed in the microstructure obtained at the highest cooling rate (i.e. at 5 mm distance from the chill, DAS ~ 15 μm). As the cooling rate decreases, the β-needles are observed in relative abundance (at 100 mm distance from the chill, DAS ~ 90 μm).

2. Sympathetic nucleation of the β-needles is observed in the unmodified alloy (at 100 mm distance from the chill), that produces large β-needle entities (comprising several branched segments) which can extend up to as much as ~ 1200 μm across the matrix surface.

3. The addition of strontium vastly reduces the phenomenon of sympathetic nucleation, through its poisoning action on the β-needle nucleation sites; this reduces the number of sites available for nucleation, and a lower β-needle density is obtained (albeit somewhat larger sized needles), compared to that in the unmodified alloy. Dissolution of the β-needles is also observed with strontium addition, resulting in fragmentation of the needles. The dissolution effect accelerates with increasing strontium level. Optimum strontium concentration is obtained at ~300 p.p.m., at which level almost 90% of the needles possess the lowest lengths (0–40 μm) compared to ~55% for the modified alloy.

4. Thickening of the β-needles is observed with grain refining, in addition to the branching effect of sympathetic nucleation. Thick needles in the grain-refined alloy undergo brittle fracture as opposed to the fragmentation that occurs in the case of modification.

5 Grain refinement of the modified alloy is seen to nullify the beneficial effect of modification in that the H1TS3 alloy displays a much larger β-needle density than the H1S3 alloy.

Acknowledgements

Financial support received from the Natural Sciences and Engineering Research Council of Canada, the Centre québécois de recherche et de développement de l'aluminium (CQRDA), and General Motors Powertrain Division is gratefully acknowledged.

References

1. A. COUTURE, *AFS Int. Cast Metals J.* December (1981) 9.
2. S. MURALI, K. S. RAMAN and K. S. S. MURTHY, *Mater. Sci. Eng.* **151A** (1992) 1.
3. O. VORREN, J. E. EVENSON and T. B. PEDERSEN, *Am. Foundrymen's Soc. Trans.* **92** (1984) 459.
4. A. M. SAMUEL and F. H. SAMUEL, *Metall. Mater. Trans.* **26A** (1995) 2359.
5. *Idem., ibid. J. Mater. Sci.* **30** (1995) 4823.
6. A. M. SAMUEL, J. GAUTHIER and F. H. SAMUEL, *Metall. Mater. Trans.* A **27A** (1996) 1785.
7. F. T. LEE, J. F. MAJOR and F. H. SAMUEL, *ibid.* **26A** (1995) 1553.
8. S. MURALI, K. S. RAMAN and K. S. S. MURTHY, *Mater. Charact.* **33** (1994) 99.
9. Y. AWANO and Y. SHIMIZU, *Am. Foundrymen's Soc. Trans.* **98** (1990) 889.
10. L. A. NARAYANAN, F. H. SAMUEL and J. E. GRUZLESKI, *Metall. Mater. Trans.* **25A** (1994) 1761.
11. W. BONSACK, *ASTM Bull.* **117** August (1942) 45.
12. C. MASCRE, *Fonderie* **108** January (1955) 4330.
13. D. L. COLWELL and R. J. KISSLING, *Am. Foundrymen's Soc. Trans.* **69** (1961) 610.
14. J. GOBRECHT, *Giesserei* **61** (10) (1975) 263.
15. D. A. GRANGER, *Am. Foundrymen 's Soc. Trans.* **99** (1991) 379.
16. M. H. MULAZIMOGLU, F. PARAY, G. STEPHEN, B. KULUNK and J. E. GRUZLESKI, in "Light Metals 1994", edited by U. Mannweiler (The Minerals, Metals and Materials Society, Warrendale, PA, 1994) pp. 1047–1056.

Received 6 February
and accepted 18 March 1996